A Single-Layer 10–30 GHz Reflectarray Antenna for the Internet of Vehicles

Long Zhang, *Member, IEEE*, Junxun Zhang, Yejun He, *Senior Member, IEEE*, Chunxu Mao, *Member, IEEE*, Wenting Li, Sai-Wai Wong, *Senior Member, IEEE*, Peng Mei, and Steven Gao, *Fellow, IEEE*

***Abstract*—A novel ultra-wideband (UWB) reflectarray antenna for the Internet of Vehicles (IoV) is introduced in this paper. By simply connecting the neighboring reflectarray elements, the proposed reflectarray antenna achieves a remarkable radiation pattern bandwidth of 20 GHz, ranging from 10 GHz to 30 GHz. To explain the operating principles of the proposed reflectarray antenna, the equivalent circuit (EQC) model of the unit cell is built, which also provides an efficient and rapid way to analyze the performance of the proposed reflectarray element. It is found from the EQC analysis that the connected elements can achieve better reflection phase responses than conventional separated elements, thereby improving the array bandwidth. As a proof of concept, a 503-element reflectarray antenna simultaneously covering the vehicle-to-satellite bands (12.25–12.75 GHz/14.0–14.5 GHz/19.6–21.2 GHz/29.4–31.0 GHz), the 24-GHz short-range vehicle radar band (24.25–26.65 GHz) and the 5G millimeter-wave band (27.5–28.35 GHz) is designed, fabricated, and characterized. The experimental results demonstrate that the presented reflectarray antenna can maintain undistorted beams, high antenna gain, low cross-pol level, and moderate aperture efficiency over a bandwidth of 100%, i.e., from 10 to 30 GHz. With its simple and planar aperture as well as excellent performance, the proposed reflectarray antenna can be a promising candidate for vehicles that require reliable high data-rate satellite links and 5G millimeter-wave connections simultaneously.**

***Index Terms*—Internet of vehicles (IoV), reflectarray antenna, ultra-wideband (UWB) arrays.**

I. Introduction

INTERNET of Vehicles (IoV) has drawn great attentions from academic and industry because of its huge research values and commercial interests over the past few years [1]. The development of the IoV can effectively alleviate or solve various problems caused by the rapid growth of vehicles, and greatly improve the transportation efficiency, safety and intelligence level [2]. One of the key technologies for the success of the IoV is building a reliable high-speed communication system. Fig. 1 shows the different communication links for the IoV. As can be seen, IoV uses a new generation of information and communication technology to realize all-round links including the vehicle-to-network (V2N), vehicle-to-vehicle (V2V), vehicle-to-pedestrian (V2P), and vehicle-to-infrastructure (V2I) [3]. To provide a safer and more coordinated transportation network, additional communication links can be used [4]. For example, satellite communication has great potential in the application of the IoV due to the advantages of wide coverage, bandwidth flexibility, and high reliability [5]. Besides, the deployment of short-range vehicle radars, and 5G communication systems on board of vehicles also contribute to the functionality of IoV [6]. Short-range vehicle radars can provide situational awareness by detecting nearby objects in the form of distance, velocity and angle information, which benefits vehicle safety for IoV [7]. Meanwhile, to enable high data rate for IoV, the 5G communication systems play a pivotal role, which can improve the system capacity, transmission scope, and spectrum efficiency [8]. As these systems work at different frequencies, normally several separate antennas need to be utilized for transmitting and receiving signals for different systems. However, this brings about several problems such as increased antenna blockage, electromagnetic interference, and reduced system capacity [9]. To solve these problems, a broadband, high-gain, and shared aperture antenna that can work at several frequency bands simultaneously is highly desired.

Reflectarray antenna has proven to be a reliable candidate for various applications due to their low profile, high gain, low cost, and simplified feeding [10] and has already been applied to automotive vehicles [11]. However, reflectarray antennas generally have narrow bandwidth due to the inherent narrowband property of the elements and the differential spatial phase delay. If an ultra-wideband (UWB) reflectarray antenna can be realized, it would be a good candidate for achieving multiple functions, such as short-range vehicle radar, 5G mobile communication, and satellite communication, within in one single radiating aperture [12], [13]. To improve the bandwidths of the reflectarray antennas, various methods have been proposed in recent years [14]–[17]. In [18] and [19], the sub-wavelength unit cells

Manuscript received May 19, 2021; revised August 27, 2021 and October 14, 2021; accepted December 2, 2021. Date of publication December 13, 2021; date of current version February 14, 2022. This work was supported in part by the National Natural Science Foundation of China under Grants 61801299 and 62071306, in part by the Natural Science Foundation of Guangdong Province under Grant 2020A1515011037, and in part by the Shenzhen Science and Technology Program under Grants JCYJ20200109113601723 and JSGG20210420091805014. The review of this article was coordinated by Prof. Mugen Peng. *(Corresponding author: Yejun He.)*

Long Zhang, Junxun Zhang, Yejun He, Wenting Li, and Sai-Wai Wong are with the College of Electronics and Information Engineering, Shenzhen University, Shenzhen 518060, China (e-mail: long.zhang@szu.edu.cn; junxunzhang@126.com; heyejun@126.com; w.li@szu.edu.cn; wongsaiwai@ieee.org).

Chunxu Mao is with the Institute for Communication Systems (ICS), 5G Innovation Centre (5GIC), University of Surrey, GU2 7XH Guildford, U.K. (e-mail: c.mao@surrey.ac.uk).

Peng Mei is with the Antennas, Propagation, and Millimeter-Wave Systems Section, Department of Electronic Systems, Aalborg University, 9220 Aalborg, Denmark (e-mail: mei@es.aau.dk).

Steven Gao is with the School of Engineering and Digital Arts, University of Kent, CT2 7NT Canterbury, U.K. (e-mail: s.gao@kent.ac.uk).

Digital Object Identifier 10.1109/TVT.2021.3134836

were employed to broaden the bandwidth of the reflectarray antennas. In [20]–[22], the single-layer multi-resonance structures were used as the unit cells to expand the gain bandwidth of the reflectarrays. The multi-resonance unit cells can generate sufficient phase shift at different frequencies, and thereby a reduced phase error was achieved, resulting in an improved bandwidth.

As the bandwidths of the conventional reflectarray antennas rarely exceed one octave, an alternative way to meet the system requirement of multi-band operation is to employ the multi-band reflectarray antennas [23]–[26]. There are several methods that can be used to achieve a multi-band reflectarray antenna, such as the adoption of sub-wavelength rectangular grids at two bands [27], the Phoenix elements [28], the FSS design techniques [29], and the unit cell with two equilateral triangular patches of different sizes [11].

To date, there are few reported works focusing on reflectarrays that can support a multi-octave bandwidth. The concept of tightly coupled dipole array (TCDA) was introduced in the design of the reflectarray antenna in [30], which demonstrated a breakthrough of 3:1 bandwidth for reflectarray design. However, non-planar array aperture and interleaved substrates are used to implement the design concept, which results in rather bulky and unreliable array configuration. In order to restore the features of the planar array aperture, robust and reliable array configuration, and low fabrication cost of the reflectarray, it is highly desirable that the multi-octave bandwidth can be achieved with a fully planar reflectarray aperture.

This paper proposes a fully planar, single-layer, linearly polarized UWB reflectarray antenna that can cover the vehicle-to-satellite bands (12.25–12.75 GHz/14.0–14.5 GHz/19.6–21.2 GHz/29.4–31.0 GHz), the 24-GHz short-range vehicle radar band (24.25–26.65 GHz) and the 5G millimeter-wave band (27.5–28.35 GHz), simultaneously. The proposed antenna can be placed on the roof of the vehicles, similar to the scenario introduced in [11]. To the best knowledge of the authors, this is the first time that a single-layer reflectarray antenna can provide continuous bandwidth coverage from the X-band to the Ka-band with a single planar array aperture. Connected dipole elements are used to constitute the proposed reflectarray, which maintains undistorted beams and high antenna gain from 10 GHz to 30 GHz. In addition, the equivalent circuit (EQC) model of the unit cell is constructed to predict the element performance quantitatively, which provides an in-depth understanding of the antenna operating principles. Furthermore, the phase errors caused by the phase center variation of the feed horn and the differential spatial phase delay are elaborately compensated to keep a good array performance. With the merits of ultra-wide bandwidth, high antenna gain, single-layer planar aperture, and low fabrication cost, the proposed reflectarray antenna can be a promising candidate for IoV application and 5G millimeter-wave connections simultaneously. In this way, the vehicles can always maintain a reliable link with the satellite, the 5G base stations, and other vehicles.

The rest of this paper is organized as follows. The unit cell design and analysis are presented in Section II. Section III presents the design and analysis of the proposed reflectarray. Simulated and measured results and comparisons with other reported wideband reflectarrays are presented and discussed in Section IV. Finally, a conclusion is drawn in Section V.

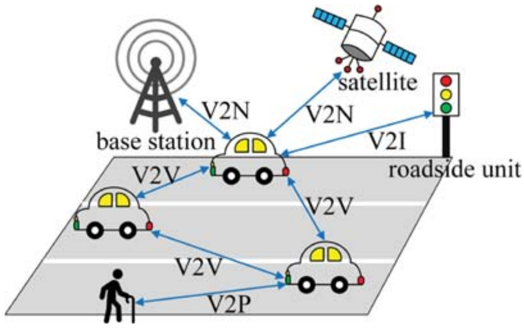

Fig. 1. Demonstration of the different communication links for the IoV.

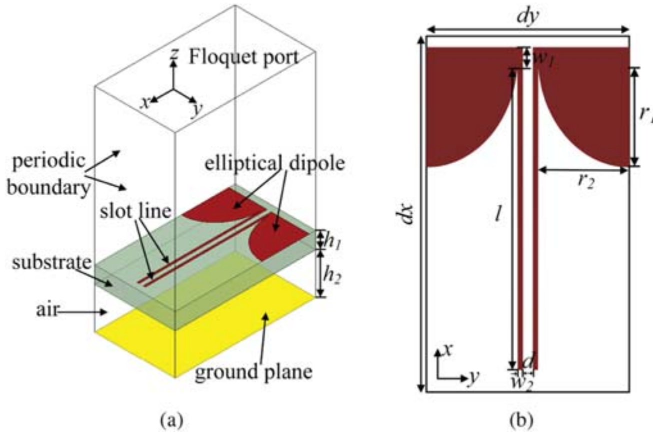

Fig. 2. Geometry of the proposed reflectarray unit cell. (a) Perspective view. (b) Top view.

II. Unit Cell Design and Analysis

A. Geometry of the Reflectarray Unit Cell

The geometry of the proposed reflectarray unit cell is illustrated in Fig. 2, which consists of an elliptical dipole, a slot line, and a ground plane. The elliptical dipole and slot line are printed on a 0.813 mm Rogers RO4003 C substrate with the relative permittivity and loss tangent of 3.55 and 0.0027, respectively. By adjusting the length l of the slot line, different phase shifts can be achieved. An air layer with a height of h_2 is introduced between the substrate and the ground plane to improve the bandwidth performance of the reflectarray. The size of the unit cell is denoted by $dx \times dy$. The value of dy is determined according to the element distance given in [30] at first, and then optimized by the EQC model. Meanwhile, dx can be acquired through EQC analysis and HFSS simulation, provided that the slot line can offer sufficient reflection phase range. Moreover, good reflection performance of the unit cell can be obtained within a wide operating band by choosing an appropriate dy and h_2. Notice that there is no gap between the dipole end and the edge of the substrate, the adjacent dipole elements of the proposed reflectarray are thus directly connected with each other. With this arrangement, the proposed reflectarray

TABLE I
GEOMETRICAL PARAMETERS OF THE REFLECTARRAY UNIT CELL (UNIT: MM)

w_1	w_2	r_1	r_2	dx	dy	h_1	h_2	d
0.2	0.1	2.1	1.75	6.8	3.9	0.813	2	0.2

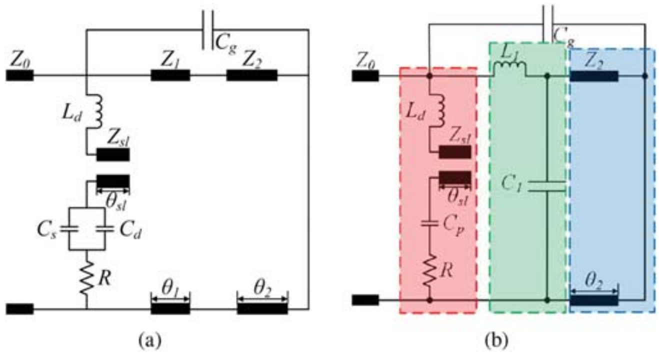

Fig. 3. EQC models of the proposed reflectarray unit cell. (a) General EQC model. (b) Simplified EQC model.

can achieve an ultra-wide bandwidth, which will be discussed subsequently.

The geometrical parameters of the dipole unit cell are shown in Table I. It is noted that the value of dy is chosen to be 3.9 mm for optimum unit cell performance, which is only 0.13λ at 10 GHz.

B. Equivalent Circuit Analysis of the Unit Cell

In order to better understand the operating principles of the proposed unit cell, an EQC model of the unit cell is established and shown in Fig. 3(a). In the EQC model, the inductor L_d and capacitor C_d in series are used to characterize the elliptical dipole, where L_d is caused by the induced current on the surface of the elliptical dipole. When the influence of the supporting dielectric substrate is considered, a shunt capacitor C_s is included to compensate the self-capacitance C_d [31]. The slot line is represented by an open-circuit transmission line with the characteristic impedance Z_{sl} and electrical length θ_{sl}. In the EQC model, the resistor R is included to represent the copper loss of the elliptical dipole and the dielectric loss of the substrate. The numerical values of L_d, C_d, C_s, and R in the equivalent circuit are individually calculated using the cascaded transmission matrices approach reported in [32] and [33]. It should be noted that the metallic ground plane is not considered when determining the values of the components in the EQC. In order to build a more accurate EQC model, the capacitance effect between the elliptical dipole and the metallic ground plane must be taken into consideration and thus a shunt capacitor C_g is included. Besides, the Rogers RO4003 C substrate and the air layer are modeled by two transmission lines, and their characteristic impedance Z_d and electric length θ_d can be calculated through the following formulas.

$$Z_d = \frac{Z_0}{\sqrt{\varepsilon_{rd}}} \tag{1}$$

TABLE II
VALUES OF THE LUMPED CIRCUIT ELEMENTS

L_d	Z_{sl}	C_d	C_s	R	C_g
1.5451nH	175ohm	0.0112pF	0.0143pF	16ohm	0.01pF

$$\beta_d = k_0\sqrt{\varepsilon_{rd}} \tag{2}$$

$$\theta_d = h_d\beta_d \tag{3}$$

where the subscript d is replaced by 1 and 2 to represent the substrate and the air layer, respectively. The characteristic impedance of the free space is denoted by Z_0, while k_0 is the free space wave number. The detailed values of each EQC component are listed in Table II.

Based on the telegrapher's equation [34], the EQC model in Fig. 3(a) can be further simplified by replacing the transmission line (Z_1, θ_1) with a series inductor $L_1 = \mu_0\mu_r h_1$ and a shunt capacitor $C_1 = \varepsilon_0\varepsilon_r h_1/2$ [35]. Notice that the transmission line (Z_2, θ_2) is shorted by the ground plane, its input impedance can be directly calculated and thus is not replaced by inductors and capacitors for simplicity.

According to the transmission line theory [34], the input impedance of the open-circuit slot line Z_s and the grounded air layer Z_{ga} can be individually expressed by

$$Z_s = -jZ_{sl}\cot\beta l \tag{4}$$

$$Z_{ga} = jZ_2\tan\beta_2 h_2 \tag{5}$$

Fig. 3(b) shows the simplified EQC model, where $C_p = C_s \| C_d$. As shown in Fig. 3(b), the EQC model of the unit cell is mainly composed of three parts which are enclosed in the three colored boxes. The circuit components in the red, green, blue box are used to describe the characteristics of the elliptical dipole and the slot line, the Rogers RO4003 C substrate, and the grounded air layer, respectively. According to the circuit topology, the input impedance of the red colored part can be calculated by

$$Z_{Dipole} = R + j\omega L_d + Z_s + \frac{1}{j\omega C_p} \tag{6}$$

By connecting the input impedances of the three parts together, the input impedance of the proposed unit cell can be calculated as

$$Z_{RA} = \left\{\left[\left(R + j\omega L_d + Z_s + \frac{1}{j\omega C_p}\right) \| \frac{1}{j\omega C_g}\right] + j\omega L_1\right\} \left\| \frac{1}{j\omega C_1} \right\| Z_{ga} \tag{7}$$

By denoting the input impedance in the complex form as $Z_{RA} = R_{RA} + jX_{RA}$, the reflection coefficient of the unit cell

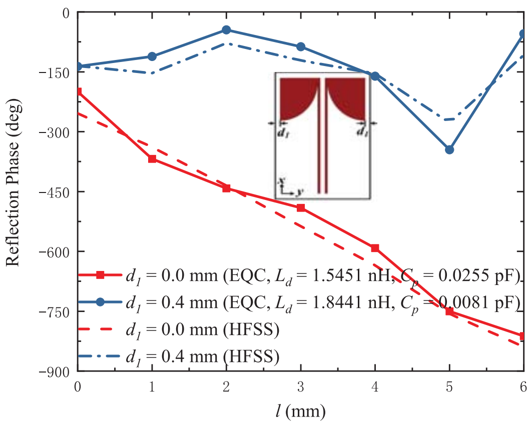

Fig. 4. Calculated results of the reflection phase versus the slot line lengths l at 28 GHz for different d_1 of the element by the EQC model and the full-wave simulation.

can then be calculated by

$$\begin{aligned} \Gamma &= |\Gamma| e^{j\angle|\Gamma|} = \frac{Z_{RA} - Z_0}{Z_{RA} + Z_0} \\ r(\omega, l) &= 20 \lg |\Gamma| \\ \angle\Gamma &= \varphi(\omega, l) = \arctan\left(\frac{2X_{RA}Z_0}{R_{RA}^2 + X_{RA}^2 - Z_0^2}\right) \end{aligned} \tag{8}$$

where r is the magnitude of the reflection coefficient, φ is the phase of the reflection coefficient, ω is the angular frequency. It is observed from (8) that both the magnitude and the phase of the reflection coefficient depend on ω and l.

To explain why the connected element configuration is selected in this work, Fig. 4 shows the reflection phase of the unit cell with different element gaps (equal to $2d_1$). As shown by the inset of Fig. 4, the distance between the dipole tip and the unit cell boundary is denoted by d_1 ($d_1 = 0$ for the proposed unit cell). From Fig. 4, it is observed that the decrease of d_1 results in better reflection phase response. When $d_1 = 0$, the slope of the reflected phase curve $p = \dfrac{\partial\varphi(\omega, l)}{\partial l}$ tends to be a nonzero constant, indicating that the reflected phase curve becomes rather linear with the increase of the slot line length l. The calculated results are validated by the full-wave simulation, demonstrating that the connected element arrangement ($d_1 = 0$) can achieve a better reflection phase response. It can be concluded from the EQC analysis that the connected element decreases the element self-inductance and increases the element self-capacitance. Consequently, good element reflection performance is maintained within an ultra-wide bandwidth. It is worth pointing out that the element performance comparison shown in Fig. 4 is conducted at 28 GHz instead of the center frequency of 20 GHz. The reason for this is that the two elements have comparable performance at center frequencies but with significant differences at other frequencies. To show the difference of the two elements, Fig. 4 provides the performance comparison at 28 GHz.

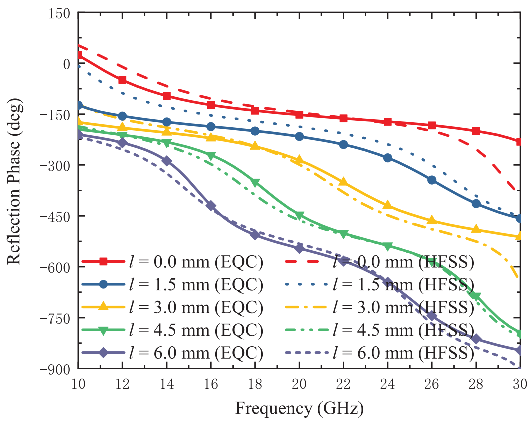

Fig. 5. Calculated reflection phases against frequency for different slot line lengths l by the EQC model and the full-wave simulation.

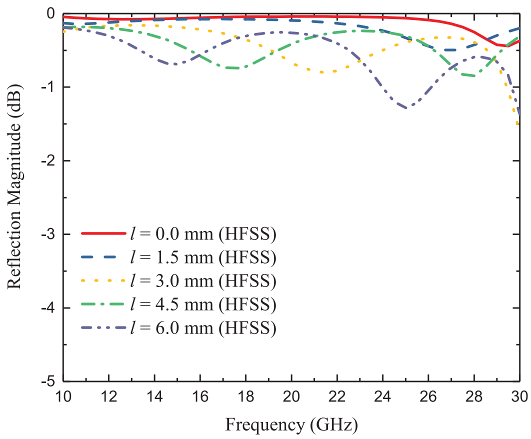

Fig. 6. Reflection magnitudes of the unit cell with different l.

C. Performance of the Reflectarray Unit Cell

The performance of the unit cell is evaluated by the EQC model and then verified by the full-wave simulation using the ANSYS HFSS. With the aid of the EQC model, the reflection performance of the unit cell can be optimized efficiently. To demonstrate the performance of the reflectarray unit cell, the reflection phases of the unit cell against frequency for different slot line lengths l are plotted in Fig. 5. As shown, the EQC results agree well with the full-wave simulation results, which verify the validity and accuracy of the proposed EQC model. Both the EQC results and the full-wave results demonstrate that the unit cell can provide sufficient phase shift over a wide frequency range. Fig. 6 shows the reflection magnitudes of the unit cell with different slot line length l. As shown in this figure, the reflection loss is smaller than 0.5 dB over the whole bandwidth when l is smaller than 1.5 mm. In other cases, the average loss of the proposed unit cell is smaller than 1 dB.

Fig. 7 shows the reflection magnitude and phase responses of the unit cell under different oblique incident angles. As shown in Fig. 7, the reflection magnitude variations are rather small under oblique incidence with the incidence angle up to 30°. Considering that the maximum incident angle from the horn to the aperture edge is smaller than 30°, the variation of the

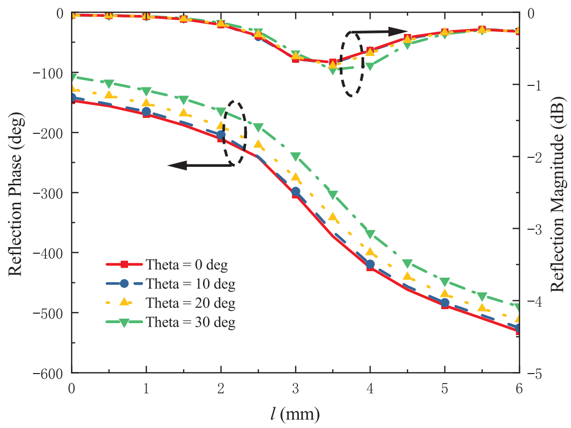

Fig. 7. Reflection magnitudes and phases of the unit cell under different oblique incident angles at 20 GHz.

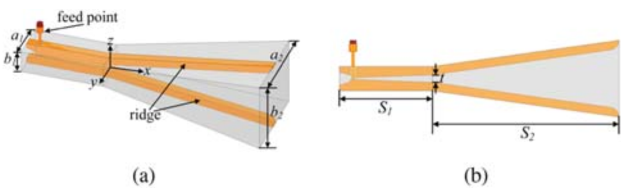

Fig. 8. Configuration of the DRHA. (a) Perspective view. (b) Side view.

TABLE III
PARAMETERS OF THE DRHA (UNIT: MM)

a_1	b_1	a_2	b_2	S_1	S_2	t
12.64	6.54	26.7	20.6	25	50	1.96

reflection phase under oblique incidence is still acceptable for most of the reflectarray elements.

III. REFLECTARRAY DESIGN AND ANALYSIS

A. Design of the Feed Antenna

To realize an UWB reflectarray, an UWB feed antenna with stable phase center is required. In this work, a double-ridged horn antenna (DRHA) is designed as the feed. The configuration of the proposed DRHA is shown in Fig. 8. As shown, two ridges are introduced to reduce the cut-off frequency of the TE_{10} mode, thereby improving the bandwidth of the horn antenna. By gradually increasing the ridge gap, a broadband impedance matching is achieved. The detailed geometry parameters of the DRHA are listed in Table III. Using the computer numerical control (CNC) machining, the DRHA is fabricated. The simulated and measured $|S_{11}|$ and realized gains of the DRHA are shown in Fig. 9. As shown, the feed horn can maintain $|S_{11}|$ <-15 dB from 10 GHz to 30 GHz. The measured realized gains are ranged from 10.14 to 17.16 dBi, which is reasonably consistent with the simulated results.

Another issue to be concerned is the DRHA's phase center, which is changed with the frequency. To minimize the phase errors, the position of the phase center $p(x, y, z)$ of the feed

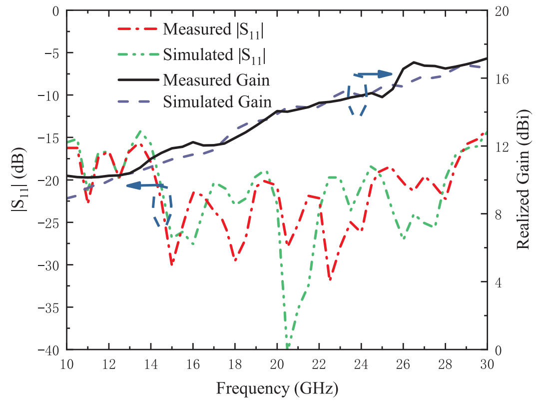

Fig. 9. Simulated and measured S_{11} and realized gains of the DRHA.

antenna is calculated using the following equation.

$$p(x, y, z) = \sum_{f=f_1}^{f_2} \frac{p_f(x, y, z)}{N} \tag{9}$$

where $p_f(x, y, z)$ denotes the position of the phase center at the frequency f and N is the number of sampling frequency points from f_1 to f_2. By using the information of $p_f(x, y, z)$ shown in Table IV, the phase center of the feed antenna can be finally determined.

B. Equivalent Distance Delay for Ultra-Wideband Phase Compensation

The concept of equivalent distance delay has been proposed in [30] and [36], which explains that the differential spatial phase delay can be compensated appropriately in a certain band if the calculated equivalent distance delay keeps unchanged within the band. For a typical reflectarray, the following equation can be used to calculate the required phase distribution over the array aperture:

$$\Phi(x_i, y_i) = -k_0 \sin\theta_b (x_i \cos\theta_b + y_i \sin\varphi_b) + R_i k_0 \tag{10}$$

where $\Phi(x_i, y_i)$ is the required phase shift of each reflectarray unit cell, k_0 is the wave number in free space, and (θ_b, φ_b) is the beam direction of the reflectarray. The position of the ith reflectarray element on the array aperture is denoted by (x_i, y_i), and the distance between the element and the phase center of the feed antenna is R_i. In order to eliminate the effects of the frequency, the (10) is divided by k_0 and rewritten as

$$\Phi(x_i, y_i)/k_0 = -\sin\theta_b (x_i \cos\theta_b + y_i \sin\varphi_b) + R_i \tag{11}$$

Let

$$d(x_i, y_i) = \Phi(x_i, y_i)/k_0 \tag{12}$$

$$d'(x_i, y_i) = d(x_i, y_i) - d(x_1, y_1) \tag{13}$$

We could obtain

$$d'(x_i, y_i) = -\sin\theta_b [(x_i - x_1)\cos\theta_b + (y_i - y_1)\sin\varphi_b] + (R_i - R_1) \tag{14}$$

TABLE IV
POSITIONS OF THE DRHA PHASE CENTER AT DIFFERENT FREQUENCIES (UNIT: MM)

Frequency (GHz)	10	12	14	16	18	20	22	24	26	28	30
$p_f(x,y,z)$	(48.7,0,0)	(48.3,0,0)	(47.5,0,0)	(47.0,0,0)	(48.6,0,0)	(47.9,0,0)	(46.9,0,0)	(44.6,0,0)	(44.7,0,0)	(44.8,0,0)	(40.7,0,0)

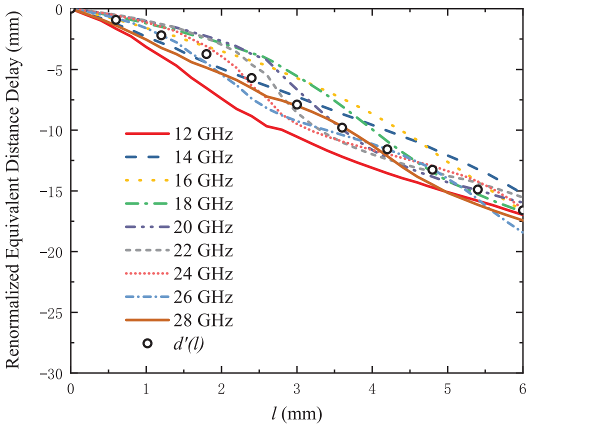

Fig. 10. Calculated renormalized equivalent distance delay of the proposed unit cell.

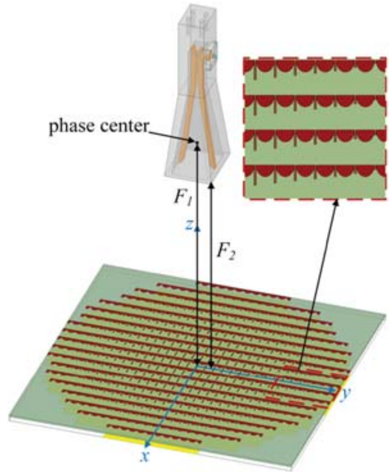

Fig. 11. Configuration of the proposed reflectarray antenna.

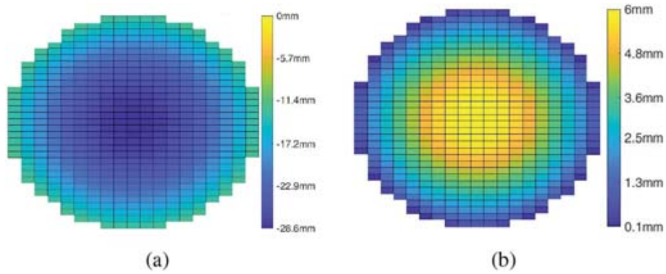

Fig. 12. Calculated element information across the array aperture. (a) Equivalent distance delay for each element. (b) Length of the slot line for each element.

where $d(x_i, y_i)$ is named as the required equivalent distance delay of the ith element, and $d'(x_i, y_i)$ is the renormalized equivalent distance delay to the corner element. As $d'(x_i, y_i)$ is independent of frequency, it can be used to compensate the differential spatial phase delay of an UWB reflectarray antenna.

The renormalized equivalent distance delay $d'(l, f)$ produced by the proposed reflectarray unit cell at different frequencies is also calculated according to (12) and (13), and demonstrated in Fig. 10, where $d'(l, f) = d(l, f) - d(l_1, f)$, $l_1 = 0$ mm. Although the renormalized equivalent distance delays of the proposed unit cell are not completely overlapped at different frequencies, the deviation is very small, indicating that the proposed element can satisfy (14) within an ultra-wide frequency range.

To minimize the phase errors over an ultra-wide frequency band, second-degree polynomial curve fitting in a least-squares sense is used to determine the design function of $d'(l)$ for the reflectarray, which is derived as follows:

$$d'(l) = -0.0648 \times l^2 - 2.5379 \times l + 0.5572 \qquad (15)$$

The curve of $d'(l)$ versus l is also included in Fig. 10 and denoted by hollow dots. By using the $d'(l)$ to design the reflectarray, reduced phase error can be obtained over an ultra-wide bandwidth. Therefore, the function $d'(l)$ is used to calculate the length l of the slot line of each reflectarray unit cell.

C. Design of the Reflectarray Antenna

As a proof of concept, a primary-fed reflectarray antenna with a diameter of 129 mm is designed by using the proposed reflectarray unit cell. The configuration of the proposed reflectarray antenna is shown in Fig. 11. As shown, 503 connected dipole elements are printed on the top-layer of the supporting substrate. An inset of the array aperture details the connection of neighboring elements. The distance between the array aperture and the DRHA aperture (denoted by F_2) is 115.5 mm, while the distance between the phase center of the DRHA and the array aperture (denoted by F_1) is 119 mm, leading to a focus/diameter (F/D) ratio of 0.92. With this F/D ratio, a proper illumination is realized and the average aperture efficiency (AE) can be improved.

The required renormalized equivalent distance delays of all reflectarray elements are calculated according to (14) and shown in Fig. 12(a). Accordingly, the required lengths of the slot lines are calculated via (15) and shown in Fig. 12(b). With this information, the array can be finalized.

IV. RESULTS AND DISCUSSION

To verify the design concept, the proposed reflectarray antenna is prototyped and fabricated, as shown in Fig. 13. A CNC machined DRHA is placed above the array aperture with the support of three plastic pillars. The radiation performance of the reflectarray is measured in an anechoic chamber, with the measurement setup shown in Fig. 14.

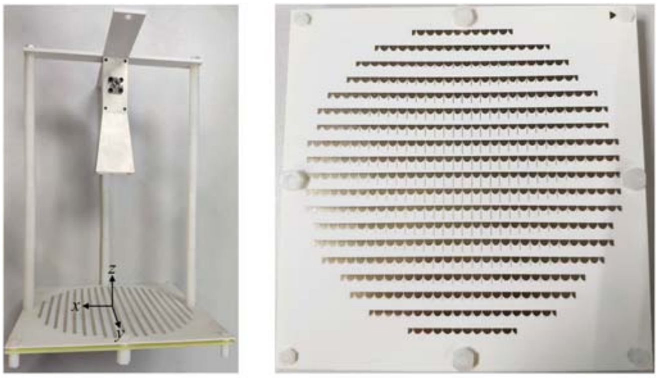

(a) (b)

Fig. 13. Prototype of the proposed reflectarray. (a) Perspective view. (b) Top view of the array aperture.

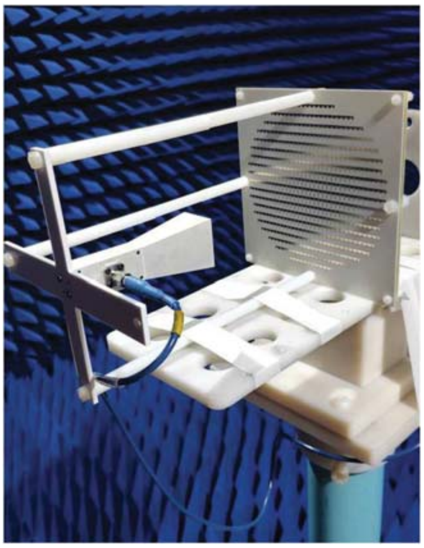

Fig. 14. Measurement setup of the proposed reflectarray.

A. Radiation Patterns

The simulated and measured normalized radiation patterns are shown in Fig. 15. To fully demonstrate the UWB performance of the proposed reflectarray, the radiation patterns are provided with a frequency step of 4 GHz. As shown, a linearly polarized well-shaped pencil beam directed in the broadside direction is obtained from 10 to 30 GHz. Within this frequency range, the radiation patterns are not distorted and good cross-pol performance is achieved. Although the proposed antenna is linearly polarized, a circularly polarized counterpart may be realized with increased complexity and cost.

The measured cross-pol levels are around -25 dB over most of the operating bands except for the low frequency region (10 GHz). It is also noted that the simulated cross-pol levels in the E-plane are rather low (<-40 dB) and thus are not shown in most of the figures. The reason for the low cross-pol levels in the E-plane is mainly attributed to the pure reflected electric fields along the direction of dipole elements (y-direction), which is caused by the connected-element configuration. This kind of element arrangement imitates the Munk's current sheet array [37], and thus continuous current is maintained along y-direction, leading to a pure radiation in y-direction. As the element is separately placed along x-direction, discrete current distribution occurs along this direction and higher cross-pol level than that of the E-plane is resulted in the H-plane (xz-plane). The rise of the measured cross-pol levels is due to the fabrication errors of the feed horn and the scattering of the cables.

The sidelobe level (SLL) is around -10 dB over majority of the bandwidth and reaches -15 dB in the middle of the band. The relatively high sidelobe level is mainly due to the phase errors over the array aperture, measurement errors, fabrication errors of the feed horn, and the scattering from the feed horn fixture and the measurement cables. With focusing on the main beam performance and the cross-pol levels, the proposed reflectarray antenna can generally maintain a stable radiation pattern and achieve an average cross-pol level of -25 dB within a 3:1 bandwidth.

B. Realized Gain and Aperture Efficiency

The simulated and measured realized gains and aperture efficiencies of the proposed reflectarray are shown in Fig. 16. It is observed that the simulated and measured realized gains generally enhance with the increase of frequency. The simulated gain varies from 15.65 to 27.12 dBi, while the measured gain ranges from 14.11 to 27.51 dBi in the operating band. The measured peak gain of 27.51 dBi is achieved at the frequency of 26 GHz.

As shown in Fig. 16, the maximum AE is 43.8% at 26 GHz based on the measurement result and 49.8% at 22 GHz according to the simulation result. By averaging the measured AE with a frequency step of 1 GHz, the measured average AE of the proposed reflectarray is about 32% from 10 to 30 GHz. It is noticed that the AE is relatively low at the lower and upper band. Generally, there are two reasons for this phenomenon. The first one is that the phase errors over the aperture at these two frequency bands are larger than that of the middle frequency band. Another factor rests on the spillover and inefficient illumination effect occurred at the edge frequencies, which is caused by the varied beamwidth feature of the feed horn over the ultra-wide bandwidth. The discrepancies between the simulation results and measurement results are due to the fabrication errors of the DRHA, the assembly errors of the antenna, and measurement errors.

C. Comparison With Other Wideband Reflectarrays

To demonstrate the merits of our work, Table V provides a comprehensive comparison between our work and other latest reported wideband reflectarray antennas in terms of array bandwidth, aperture size, aperture height, fabrication and assembly difficulty, peak gain, peak aperture efficiency, average aperture efficiency, average cross-pol level, and the bandwidth improvement method. It should be mentioned that the bandwidth definitions used in these works are not exactly the same. From the Table V, it is noted that the fractional bandwidth of the proposed reflectarray is 100%, i.e., from 10 to 30 GHz, which is much wider than other works except for [30]. Compared with the

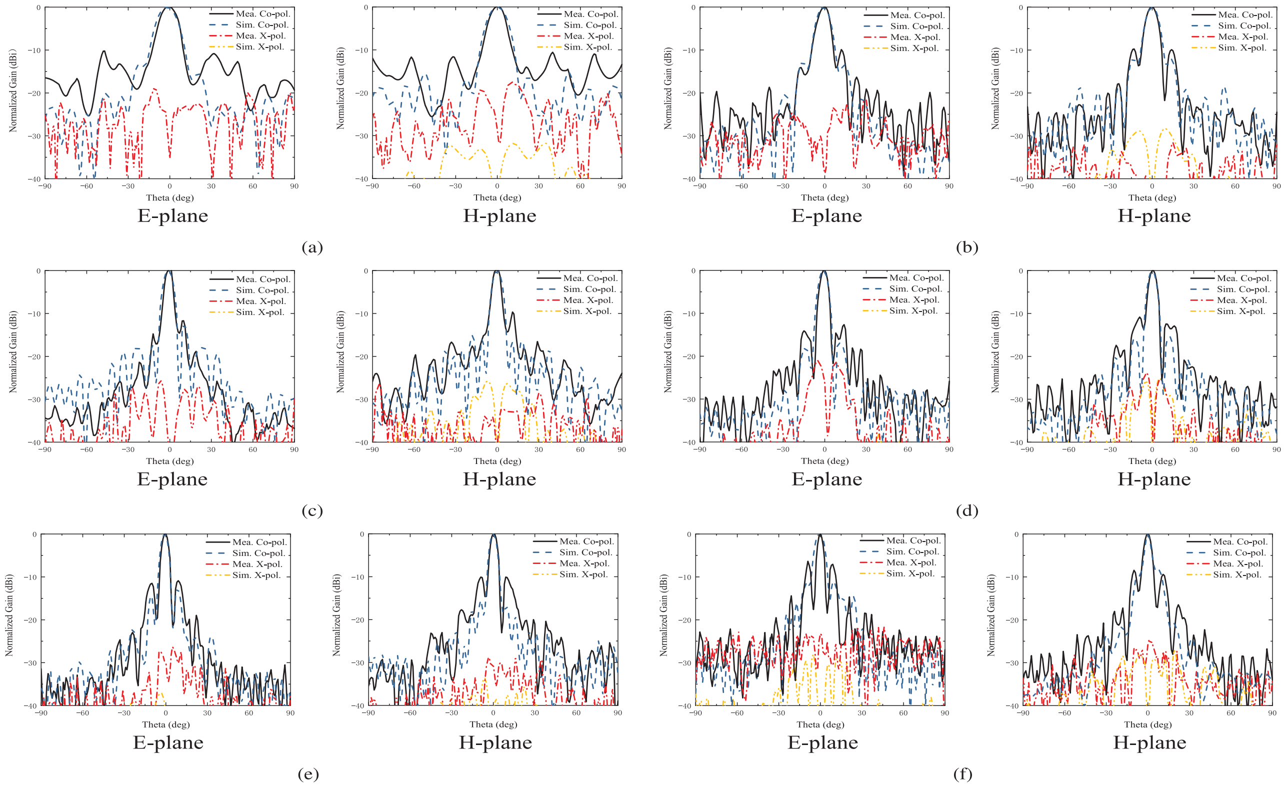

Fig. 15. Simulated and measured normalized radiation patterns of the proposed reflectarray antenna. (a) 10 GHz. (b) 14 GHz. (c) 18 GHz. (d) 22 GHz. (e) 26 GHz. (f) 30 GHz.

TABLE V
COMPARISON OF THE PROPOSED REFLECTARRAY WITH OTHER REPORTED WIDEBAND REFLECTARRAY DESIGNS

Reference No.	Bandwidth	Aperture Size (mm)(electrical size at center freq.) and Shape	Aperture Profile (mm) (electrical size at center freq.)	Fabrication and Assembling Difficulty	Measured Peak Gain (dBi)	Measured Peak AE (%)	Average AE (%)	Average Cross-Pol Level (dB)	Bandwidth Improvement Method
[15]	1-dB gain: 12.94% (39.5-45 GHz)	Φ140.4(19.89λ), Circular	1.016(0.14λ)	Moderate	32.83	51.18	44	-30.1	Using substrate integrated coaxial true-time delay lines
[16]	3-dB gain: 38.5% (9.24-13.64 GHz)	Φ266(8.87λ), Octagonal	2.8(0.11λ)	Simple	26	50	-	-26	Spiral-shaped phase delay lines
[17]	3-dB gain: 37.4% (8.7-12.7 GHz)	288 $\times$ 288(9.6λ $\times$ 9.6λ), Square	5.1(0.18λ)	Simple	24.2	20	17	-20	Exploiting the polarization rotating unit cell
[24]*	3-dB gain: 33% (6.85-9.55 GHz)/30% (11.22-15.18 GHz)	Φ250(9.6λ/11λ), Circular	6.813(0.19λ/0.3λ)	Simple	23.4/25.7	46.7/33	-	-25	Multi-resonance element
[27]*	1.5-dB gain: 24% (10.7-12.7 GHz)/21% (12.7-14.7 GHz)	408 $\times$ 399(15.91λ $\times$ 15.56λ/18.63$\lambda$$\times$ 18.22λ), Rectangular	2.2(0.09λ/0.1λ)	Simple	31.8/32.1	48/38	-	-27	Using the subwavelength patch element
[30]	Stable radiation pattern: 103% (3.4-10.6 GHz)	210 $\times$ 210(4.9λ $\times$ 4.9λ), Square	34.8(0.812λ)	Complex	22.6	38	25	-20	Tightly coupled element
This work	Stable radiation pattern: 100% (10-30 GHz)	Φ129(8.6λ), Circular	2.813(0.187λ)	Simple	27.51	43.8	32	-25	Connected planar dipole element

*Dual-band reflectarray.

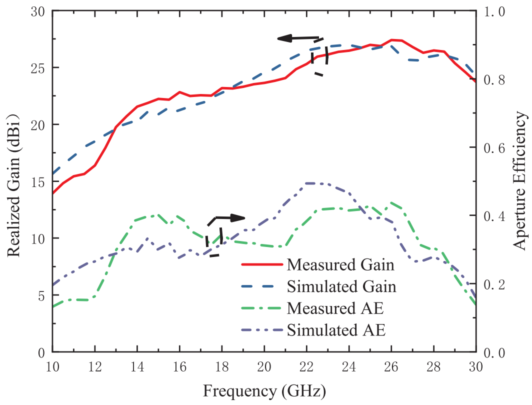

Fig. 16. Simulated and measured realized gains and aperture efficiencies of the proposed reflectarray.

design in [30], this work shows higher aperture efficiency and antenna gain, lower cross-pol level, and much simpler configuration. In addition, the aperture profile of the presented work is only about one fifth $(0.187\lambda/0.812\lambda)$ of that in [30]. Moreover, the single-layer fully planar array aperture not only greatly reduces the fabrication difficulty and cost but also notably improves the reliability and robustness of the whole reflectarray system.

V. Conclusion

In this paper, a novel UWB reflectarray antenna for IoV application has been presented. The presented reflectarray works from 10 GHz to 30 GHz with stable radiation pattern and high antenna gain, thus can cover the vehicle-to-satellite bands (12.25-12.75 GHz/14.0-14.5 GHz/19.6-21.2 GHz/29.4-31.0 GHz), the 24-GHz short-range vehicle radar band (24.25-26.65 GHz), and the 5G millimeter-wave band (27.5-28.35 GHz), simultaneously. Moreover, the proposed reflectarray can also achieve an average aperture efficiency around 32% and a cross-pol level of -25 dB across the whole bandwidth. All these merits are achieved by a single-layer fully planar aperture which is comparable to conventional reflectarrays in terms of fabrication complexity and cost. In addition, the equivalent circuit method is proposed to predict the element performance quantitatively, which helps reveal the antenna operating principles and facilitates the array design. With its ultra-wide bandwidth, high antenna gain, low cross-pol level, and low fabrication complexity and cost, the proposed reflectarray antenna would be a promising candidate for IoV application and 5G millimeter-wave connections simultaneously.

References

[1] C. Chen, J. Wu, H. Lin, W. Chen, and Z. Zheng, "A secure and efficient blockchain-based data trading approach for internet of vehicles," *IEEE Trans. Veh. Technol.*, vol. 68, no. 9, pp. 9110–9121, Sep. 2019.

[2] Z. Tian, X. Gao, S. Su, J. Qiu, X. Du, and M. Guizani, "Evaluating reputation management schemes of internet of vehicles based on evolutionary game theory," *IEEE Trans. Veh. Technol.*, vol. 68, no. 6, pp. 5971–5980, Jun. 2019.

[3] J. Wang, C. Jiang, Z. Han, Y. Ren, and L. Hanzo, "Internet of vehicles: Sensing-aided transportation information collection and diffusion," *IEEE Trans. Veh. Technol.*, vol. 67, no. 5, pp. 3813–3825, May 2018.

[4] S. Al-Sultan, A. H. Al-Bayatti, and H. Zedan, "Context-aware driver behavior detection system in intelligent transportation systems," *IEEE Trans. Veh. Technol.*, vol. 62, no. 9, pp. 4264–4275, Nov. 2013.

[5] Y. Jung, S. Eom, and S. Jeon, "Novel antenna system design for satellite mobile multimedia service," *IEEE Trans. Veh. Technol.*, vol. 59, no. 9, pp. 4237–4247, Nov. 2010.

[6] R. Singh, D. Saluja, and S. Kumar, "R-Comm: A traffic based approach for joint vehicular radar-communication," *IEEE Trans. Intell. Veh.*, to be published, doi: 10.1109/TIV.2021.3074389.

[7] Y. Won, C. Kim, and S. Lee, "Range resolution improvement of a 24 GHz ISM band pulse radar-a feasibility study," *IEEE Sensors J.*, vol. 15, no. 12, pp. 7142–7149, Dec. 2015.

[8] G. Yang and S. Zhang, "A dual-band shared-aperture antenna with wide-angle scanning capability for mobile system applications," *IEEE Trans. Veh. Technol.*, vol. 70, no. 5, pp. 4088–4094, May 2021.

[9] G. C. Tavik *et al.*, "The advanced multifunction RF concept," *IEEE Trans. Microw. Theory Techn.*, vol. 53, no. 3, pp. 1009–1020, Mar. 2005.

[10] P. Nayeri, F. Yang, and A. Z. Elsherbeni, *Reflectarray Antennas: Theory, Designs, and Applications*. New York, NY: USA: Wiley, 2018.

[11] Q. Luo *et al.*, "Multibeam dual-circularly polarized reflectarray for connected and autonomous vehicles," *IEEE Trans. Veh. Technol.*, vol. 68, no. 4, pp. 3574–3585, Apr. 2019.

[12] Q. Wu, Y. Zhou, and S. Guo, "An L-sleeve L-monopole antenna fitting a shark-fin module for vehicular LTE, WLAN, and car-to-car communications," *IEEE Trans. Veh. Technol.*, vol. 67, no. 8, pp. 7170–7180, Aug. 2018.

[13] M. G. N. Alsath *et al.*, "An integrated Tri-Band/UWB polarization diversity antenna for vehicular networks," *IEEE Trans. Veh. Technol.*, vol. 67, no. 7, pp. 5613–5620, Jul. 2018.

[14] L. Zhang, S. Gao, Q. Luo, W. Li, Y. He, and Q. Li, "Single-layer wideband circularly polarized high-efficiency reflectarray for satellite communications," *IEEE Trans. Antennas Propag.*, vol. 65, no. 9, pp. 4529–4538, Sep. 2017.

[15] Z. Miao and Z. Hao, "A wideband reflectarray antenna using substrate integrated coaxial true-time delay lines for QLink-Pan applications," *IEEE Antennas Wireless Propag. Lett.*, vol. 16, pp. 2582–2585, 2017.

[16] C. Han, Y. Zhang, and Q. Yang, "A broadband reflectarray antenna using triple gapped rings with attached phase-delay lines," *IEEE Trans. Antennas Propag.*, vol. 65, no. 5, pp. 2713–2717, May 2017.

[17] H. Luyen, Z. Yang, M. Gao, J. H. Booske, and N. Behdad, "A Wideband, Single-layer reflectarray exploiting a polarization rotating unit cell," *IEEE Trans. Antennas Propag.*, vol. 67, no. 2, pp. 872–883, Feb. 2019.

[18] P. Qin, Y. J. Guo, and A. R. Weily, "Broadband reflectarray antenna using subwavelength elements based on double square meander-line rings," *IEEE Trans. Antennas Propag.*, vol. 64, no. 1, pp. 378–383, Jan. 2016.

[19] L. Guo, P. Tan, and T. Chio, "On the use of single-layered subwavelength rectangular patch elements for broadband folded reflectarrays," *IEEE Antennas Wireless Propag. Lett.*, vol. 16, pp. 424–427, 2017.

[20] A. Vosoogh, K. Keyghobad, A. Khaleghi, and S. Mansouri, "A high efficiency ku-band reflectarray antenna using single-layer multiresonance elements," *IEEE Antennas Wireless Propag. Lett.*, vol. 13, pp. 891–894, 2014.

[21] G. Wu, S. Qu, S. Yang, and C. H. Chan, "Broadband, Single-layer dual circularly polarized reflectarrays with linearly polarized feed," *IEEE Trans. Antennas Propag.*, vol. 64, no. 10, pp. 4235–4241, Oct. 2016.

[22] M. E. Bialkowski and K. H. Sayidmarie, "Investigations into phase characteristics of a single-layer reflectarray employing patch or ring elements of variable size," *IEEE Trans. Antennas Propag.*, vol. 56, no. 11, pp. 3366–3372, Nov. 2008.

[23] E. M.-de-Rioja and J. A. Encinar, "Dual polarized reflectarray transmit antenna for operation in ku- and ka-bands with independent feeds," *IEEE Trans. Antennas Propag.*, vol. 65, no. 6, pp. 3241–3246, Jun. 2017.

[24] Z. H. Zarghani and Z. Atlasbaf, "A new broadband single-layer dual-band reflectarray antenna in X- and Ku-bands," *IEEE Antennas Wireless Propag. Lett.*, vol. 14, pp. 602–605, 2015.

[25] R. Deng, F. Yang, S. Xu, and M. Li, "An FSS-Backed 20/30-GHz dual-band circularly polarized reflectarray with suppressed mutual coupling and enhanced performance," *IEEE Trans. Antennas Propag.*, vol. 65, no. 2, pp. 926–931, Feb. 2017.

[26] S. Qu, S. Lu, C. Ma, and S. Yang, "K/Ka dual-band reflectarray subreflector for ring-focus reflector antenna," *IEEE Antennas Wireless Propag. Lett.*, vol. 18, no. 8, pp. 1567–1571, Aug. 2019.

[27] L. Guo, P. Tan, and T. Chio, “Single-layered broadband dual-band reflectarray with linear orthogonal polarizations,” *IEEE Trans. Antennas Propag.*, vol. 64, no. 9, pp. 4064–4068, Sep. 2016.

[28] R. Deng, S. Xu, F. Yang, and M. Li, “Single-layer dual-band reflectarray antennas with wide frequency ratios and high aperture efficiencies using phoenix elements,” *IEEE Trans. Antennas Propag.*, vol. 65, no. 2, pp. 612–622, Feb. 2017.

[29] R. Deng, S. Xu, F. Yang, and M. Li, “An FSS-Backed ku/ka quad-band reflectarray antenna for satellite communications,” *IEEE Trans. Antennas Propag.*, vol. 66, no. 8, pp. 4353–4358, Aug. 2018.

[30] W. Li, S. Gao, L. Zhang, Q. Luo, and Y. Cai, “An ultra-wide-band tightly coupled dipole reflectarray antenna,” *IEEE Trans. Antennas Propag.*, vol. 66, no. 2, pp. 533–540, Feb. 2018.

[31] P. Mei, S. Zhang, X. Q. Lin, and G. F. Pedersen, “Design of an absorptive fabry-perot polarizer and its application,” *IEEE Antennas Wireless Propag. Lett.*, vol. 18, no. 7, pp. 1352–1356, Jul. 2019.

[32] M. Joozadani and M. Amirhosseini, “Wideband absorber with combination of plasma and resistive frequency selective surface,” *IEEE Trans. Plasma Sci.*, vol. 44, no. 12, pp. 3254–3261, Dec. 2016.

[33] F. Costa, A. Monorchio, and G. Manara, “Efficient analysis of frequency-selective surfaces by a simple equivalent-circuit model,” *IEEE Antennas Propag. Mag.*, vol. 54, no. 4, pp. 35–48, Aug. 2012.

[34] D. M. Pozar, *Microwave Engineering*, 4th ed. New York, NY, USA: Wiley, 2012.

[35] A. Ebrahimi, Z. Shen, W. Withayachumnankul, S. F. Al-Sarawi, and D. Abbott, “Varactor-tunable second-order bandpass frequency-selective surface with embedded bias network,” *IEEE Trans. Antennas Propag.*, vol. 64, no. 5, pp. 1672–1680, May 2016.

[36] Y. Cai *et al.*, “A novel ultrawideband transmitarray design using tightly coupled dipole elements,” *IEEE Trans. Antennas Propag.*, vol. 67, no. 1, pp. 242–250, Jan. 2019.

[37] B. A. Munk, *Finite Antenna Arrays and FSS*. New York, NY, USA: Wiley, 2003.

Long Zhang (Member, IEEE) received the B.S. and M.S. degrees in electrical engineering from the Huazhong University of Science and Technology, Wuhan, China, in 2009 and 2012, respectively, and the Ph.D. degree in electronic engineering from the University of Kent, Canterbury, U.K, in 2017. From January 2018 to April 2018, he was a Research Fellow with the Poly-Grames Research Center, Polytechnique Montreal, QC, Canada. He is currently an Assistant Professor with the College of Electronics and Information Engineering, Shenzhen University, Shenzhen, China. His current research interests include circularly polarized antennas and arrays, mm-wave antennas and arrays, tightly coupled arrays, reflectarrays, and characteristic mode theory. Dr. Zhang was the TPC Member and Session Chair for several international conferences. He is a Reviewer for several technique journals, including IEEE TRANSACTIONS ON ANTENNAS AND PROPAGATION, IEEE ANTENNAS AND WIRELESS PROPAGATION LETTERS, etc.

Junxun Zhang received the M.S. degree in communication engineering from Shenzhen University, Shenzhen, Guangdong, China, in 2021. His current research interests include reflectarray antennas and base station antennas.

Yejun He (Senior Member, IEEE) received the Ph.D. degree in information and communication engineering from the Huazhong University of Science and Technology (HUST), Wuhan, China, in 2005. From 2005 to 2006, he was a Research Associate with the Department of Electronic and Information Engineering, The Hong Kong Polytechnic University, Hong Kong. From 2006 to 2007, he was a Research Associate with the Department of Electronic Engineering, Faculty of Engineering, The Chinese University of Hong Kong, Hong Kong. In 2012, he was a Visiting Professor with the Department of Electrical and Computer Engineering, University of Waterloo, Waterloo, ON, Canada. From 2013 to 2015, he was an Advanced Visiting Scholar (Visiting Professor) with the School of Electrical and Computer Engineering, Georgia Institute of Technology, Atlanta, GA, USA. Since 2011, he has been a Full Professor with the College of Electronics and Information Engineering, Shenzhen University, Shenzhen, China, where he is currently the Director of the Guangdong Engineering Research Center of Base Station Antennas and Propagation, and the Director of the Shenzhen Key Laboratory of Antennas and Propagation. He has authored or coauthored more than 200 research articles and books (chapters). He holds about 20 patents. His research interests include wireless communications, antennas, and radio frequency. Dr. He is a fellow of IET and the Chair of the IEEE Antennas and Propagation Society-Shenzhen Chapter. He was selected as a Pengcheng Scholar Distinguished Professor, Shenzhen. He was the recipient of the Shenzhen Overseas High-Caliber Personnel Level B (Peacock Plan Award B) and Shenzhen High-Level Professional Talalent (Local Leading Talent). He was the recipient of the Shenzhen Science and Technology Progress Award, and the Guangdong Provincial Science and Technology Progress Award. He is currently an Associate Editor for IEEE TRANSACTIONS ON ANTENNAS AND PROPAGATIONN, IEEE ANTENNAS AND PROPAGATION MAGZINE, IEEE NETWORK, *International Journal of Communication Systems*, *China Communications*, and *Wireless Communications and Mobile Computing*. He was the General Chair for IEEE ComComAp 2019 and the TPC Chair for IEEE ComComAp2021. He was a Reviewer for various journals, such as IEEE TRANSACTIONS ON VEHICULAR TECHNOLOGY, IEEE TRANSACTIONS ON COMMUNICATIONS, IEEE TRANSACTIONS ON WIRELESS COMMUNICATIONS, IEEE TRANSACTIONS ON INDUSTRIAL ELECTRONICS, IEEE TRANSACTIONS ON ANTENNAS AND PROPAGATION, IEEE ANTENNAS AND WIRELESS PROPAGATION LETTERS, IEEE WIRELESS COMMUNICATIONS, IEEE COMMUNICATIONS LETTERS, IEEE JOURNAL ON SELECTED AREAS IN COMMUNICATIONS, *International Journal of Communication Systems*, *Wireless Communications and Mobile Computing, and Wireless Personal Communications*. He was a Technical Program Committee Member or a Session Chair for various conferences, including the IEEE Global Telecommunications Conference (GLOBECOM), the IEEE International Conference on Communications (ICC), the IEEE Wireless Communication Networking Conference (WCNC), the IEEE Vehicular Technology Conference (VTC), the IEEE International Symposium on Antennas and Propagation (APS), the European Conference on Antennas and Propagation (EuCAP), and the Asia-Pacific Microwave Conference (APMC). He is the Principal Investigator for over 30 current or finished research projects, including NSFC of China, the Science and Technology Program of Guangdong Province,and also the Science and Technology Program of Shenzhen City.

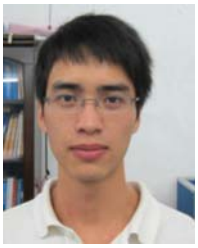

Chunxu Mao (Member, IEEE) received B.S. degree in communication engineering from the Guilin University of Electronic and Technology, Guilin, China, in 2010, the M.E. degree in RF and microwave engineering from the South China University of Technology, Guangzhou, China, in 2013, and the Ph.D. degree in electronic engineering from the University of Kent, Canterbury, U.K. in 2018. From January 2018 to August 2019, Dr. Mao was a Research Fellow with the Computational Electromagnetics and Antennas Research Laboratory (CEARL), Pennsylvania State University, State College, PA, USA. From September 2019, he joined the Institute for Communication Systems (ICS), Home of the 5G Innovation Centre (5GIC), University of Surrey, Guildford, U.K., as a Senior Research Fellow. Dr. Mao was a Session Chair in APS 2019, Atlanta. Dr. Mao was the recipient of the Outstanding Master Thesis Award of Guangdong Province, China, in 2014. Dr. Mao is Peer Reviewer in tens of journals, including IEEE TRANSACTIONS ON ANTENNAS AND PROPAGATION, IEEE TRANSACTIONS ON MICROWAVE THEORY AND TECHNIQUES, IEEE ANTENNAS WIRELESS PROPAGATION LETTERS, etc. His research interests include filtering antenna integration, metamaterial antenna, satellite antenna array, millimetre-wave antenna, and wearable antenna.

Wenting Li received the B.S. degree in electronic information engineering and the M.S. degree in electromagnetic field and microwave technology from Northwestern Polytechnical University, Xi’an, China, in 2011 and 2014, respectively, and the Ph.D. degree in electronic engineering from the University of Kent, Canterbury, U.K, in 2018. He is currently an Assistant Professor with the College of Electronics and Information Engineering, Shenzhen University, Shenzhen, China. His current research interests include reflectarray antennas, reconfigurable antennas, circularly polarized antennas, and multibeam antennas.

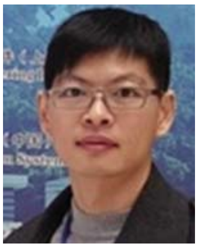

Sai-Wai Wong (Senior Member, IEEE) received the B.S degree in electronic engineering from the Hong Kong University of Science and Technology, Hong Kong, in 2003, and the M.Sc. and Ph.D. degrees in communication engineering from Nanyang Technological University, Singapore, in 2006 and 2009, respectively. From July 2003 to July 2005, he was an Electronic Engineer to lead an Electronic Engineering Department in China with two Hong Kong manufacturing companies. From May 2009 to October 2010, he was a Research Fellow with the ASTAR Institute for Infocomm Research, Singapore. Since 2010, he has been an Associate Professor and later become a Full Professor, with the School of Electronic and Information Engineering, South China University of Technology, Guangzhou, China. From July 2016 to September 2016, he was a Visiting Professor with the City University of Hong Kong, Hong Kong. Since 2017, he has been a Full Professor with the College of Electronics and Information Engineering, Shenzhen University, Shenzhen, China. He has authored or coauthored more than 200 papers in international journals and conference proceeding. His current research interests include RF/microwave circuit and antenna design.

He was the recipient of the New Century Excellent Talents in University awarded by the Ministry of Education of China in 2013, and the Shenzhen Overseas High-Caliber Personnel Level C in 2018.

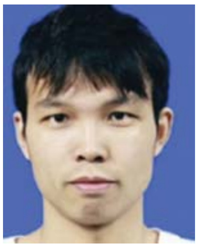

Peng Mei received the B.Eng. and M.Eng. degrees (Hons.) in electromagnetic field and microwave technology from the University of Electronic Science and Technology of China (UESTC), Chengdu, China, in 2015 and 2018, respectively. He is currently working toward the Ph.D. degree with the Antennas, Propagation and Millimeter-wave Systems section, Department of Electronic Systems, Aalborg University, Aalborg, Denmark. His current research interests include periodic structures, metasurfaces, millimeter-wave multibeam antennas, and reflectarray or transmitarray antennas. He was the recipient of the Outstanding Student of UESTC (only ten awardees every year of UESTC) in 2017, the Excellent Graduate Student of UESTC in 2018, the Excellent Graduate Student of Sichuan Province in 2018, and the Excellent Master Thesis from the Chinese Institute of Electronics in 2019. In September 2019, he was the Section Chair in IEEE-APS Topical Conference on Antennas and Propagation in Wireless Communications, held in Granada, Spain.

Steven Gao (Fellow, IEEE) received the Ph.D. degree from Shanghai University, Shanghai, China, in 1999. He is currently a Professor and the Chair of RF and Microwave Engineering, and the Director of Post-Graduate Research with the School of Engineering and Digital Arts, University of Kent, Canterbury, U.K. He has coedited or coauthored three books including *Space Antenna Handbook* (Wiley, 2012), *Circularly Polarized Antennas* (Wiley-IEEE, 2014), *LowCost Smart Antennas* (Wiley, 2019), and more than 300 articles. He holds eight patents. His current research interests include smart antenna, phased array, multi-in multi-out (MIMO), broadband and multiband antennas, small antennas, RF front ends, FSS, and their applications into 5G mobile communications, satellite communication, small satellites, radars, energy harvesting, and medical systems. Dr. Gao is a Fellow of the Royal Aeronautical Society and the IET. He was the recipient of the 2016 IET Premium Award for the Best Paper in IET Microwave, Antennas and Propagation, and the 2017 CST University Publication Award for an article in IEEE TRANSACTIONS ON ANTENNAS AND PROPAGATION. He was the General Chair of the 2013 Loughborough Antenna and Propagation Conference. He is an Associate Editor of several journals including IEEE TRANSACTIONS ON ANTENNAS AND PROPAGATION, Radio Science, *Electronics Letters*, IEEE ACCESS, and *IET Circuits, Devices and Systems*, the Editor-in-Chief of Wiley Book Series on *Microwave and Wireless Technologies*, an Editorial Board Member of many international journals, the Guest Editor of PROCEEDINGS OF THE IEEE for Special Issue on Small Satellites in 2018, the Guest Editor of IEEE TRANSACTIONS ON ANTENNAS AND PROPAGATION for Special Issue on Antennas for Satellite Communication in 2015, and the Guest Editor of *IET Circuits*, *Devices and Systems* for Special Issue in Photonic and RF Communications Systems in 2014. He was a Distinguished Lecturer of the IEEE Antennas and Propagation Society. He was an invited Speaker at many international conferences.